Topological sound in nonreciprocal active-liquid networks

Minqi Cheng,[1,*] Jingming Chen,[1,*] Linyun Yang,[2,†] and Zhen Gao[1,‡]
[1]State Key Laboratory of Optical Fiber and Cable Manufacturing Technology, Department of Electronic and Electrical Engineering, Guangdong Key Laboratory of Integrated Optoelectronics Intellisense, Southern University of Science and Technology, Shenzhen 518055, China
[2]College of Aerospace Engineering, Chongqing University, Chongqing 400030, China

(Received 12 June 2024; accepted 3 September 2025; published 1 October 2025)

Recent advances in nonreciprocal topological networks have discovered a type of anomalous topological edge states with superior robustness against larger disorders than the quasienergy band gap. However, to date, all previously demonstrated nonreciprocal topological networks have required external drives such as magnetic fields or time modulation to break the time-reversal symmetry (TRS). Here, by extending this concept to topological active matter systems with spontaneous TRS breaking, we demonstrate robust acoustic anomalous and Chern edge states in a self-propelled nonreciprocal active-liquid network without any external drives. More interestingly, we show that the anomalous topological edge states exhibit superior robustness against Hermitian disorders even than the Chern ones. Furthermore, we discover that such superior robustness no longer holds in the presence of non-Hermitian perturbations, and both the anomalous and Chern edge states transition to the corner skin modes by the non-Hermitian skin effect. Our work extends the nonreciprocal topological networks to active matter and non-Hermitian systems, offering possibilities for sound manipulation in a highly unusual way.

DOI: 10.1103/rvkr-7mr2

I. INTRODUCTION

Since the discovery of topological phases of matter [1–3], topological robustness against disorder and defects has played a central role in condensed matter physics and its classical analogs, such as photonics [4–6], acoustics [7–10], mechanics [11–13], electric circuits [14–16], and thermal diffusions [17,18]. In general, topological phases of matter can be classified into two distinct categories depending on whether their time-reversal symmetry (TRS) is invariant or not. The former includes quantum spin Hall or quantum valley Hall insulators supporting reciprocal topological edge states, which are only robust against perturbations preserving relevant symmetries, thus providing inherently weak topological protection [5,19–21]. In stark contrast, the latter includes quantum Hall or quantum anomalous Hall insulators, also well known as Chern insulators (CI) that support nonreciprocal chiral edge states (CESs), offering strong topological protections as they break the reciprocity and guarantee genuine backscattering immunity for almost any perturbations that are smaller than the Chern band gap [4,22–25].

Recently, nonreciprocal topological networks [26–31] with highly robust anomalous topological edge states, which can survive larger disorders than the quasienergy band gap and are even more reliable than the Chern ones, have been theoretically proposed and experimentally demonstrated, providing unprecedented strong topological protection against imperfections or disorders for wave manipulations. However, so far, all previous studies on nonreciprocal topological networks require external drives such as magnetic fields [26,27] or time modulation [28] to break the TRS, to some extent limiting their practical applications. Therefore, removing the requirement for external drives in nonreciprocal topological networks is highly desirable.

On the other hand, topological active matters [32] or active liquids [33,34] that are composed of self-propelled particles flowing spontaneously with TRS breaking in the absence of any external drives, have provided an ideal platform for robust sound [35–38] and cargo [39] transport. For instance, using Lieb lattices of annular channels filled with spontaneously flowing active liquids, topological active-liquid Chern insulators supporting acoustic CESs have been demonstrated [35]. However, this configuration is less suitable for realizing topological nonreciprocal active-liquid networks because the essential phase-delay link channels are absent. More significantly, it is still an open question whether a uniform steady chiral flow can be preserved in each annulus of an active-liquid network once the closed annular channels are opened and coupled by bidirectional links.

In this work, by extending the nonreciprocal topological networks to active matter system, we report topological sound manipulation in a nonreciprocal active-liquid network composing a honeycomb lattice of annular channels filled with self-propelled liquids that can flow spontaneously in the absence of any external drives. We demonstrate that such a

*These authors contributed equally to this work.
†Contact author: yanglinyun@cqu.edu.cn
‡Contact author: gaoz@sustech.edu.cn

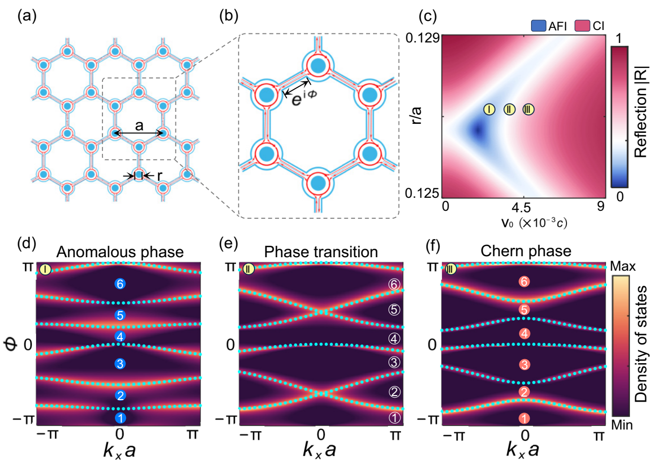

FIG. 1. Topological nonreciprocal active-liquid network. (a) Schematic of the topological nonreciprocal active-liquid network composing a honeycomb lattice of annular channels (blue color) filled with spontaneously flowing active liquid (red arrows). (b) The steady state of the active liquid was simulated using a particle-based model with red arrows representing the velocity field. ϕ represents the reciprocal phase delay imparted by the links between adjacent annuli. (c) Phase diagram of the topological nonreciprocal active-liquid network in the parameter space (v_0, r). The blue (pink) region corresponds to the anomalous (Chern) phase and the white region represents the phase transition. Floquet band structures of the (d) AFI phase ($v_0 = 0.0023c,\ r = 0.1271a$), (e) topological phase transition point ($v_0 = 0.0035c,\ r = 0.1271a$), and (f) CI phase ($v_0 = 0.0049c,\ r = 0.1271a$), corresponding to the three yellow dots in panel (c). The quasienergy band gaps are marked with numbers.

nonreciprocal topological active-liquid network can support acoustic anomalous Floquet insulator (AFI) or Chern insulator phases, depending on the individual reflection coefficient of the three-port nonreciprocal scatterers. Interestingly, we show that the acoustic AFI phase exhibits superior robustness against Hermitian disorders even stronger than the acoustic CI one. Moreover, we discover that both the acoustic AFI and CI edge states cannot survive under large non-Hermitian perturbations and transition to corner skin modes via the non-Hermitian skin effect (NHSE) [40–42].

II. CHERN AND ANOMALOUS PHASES IN AN ACTIVE-LIQUID NETWORK

We start with a honeycomb lattice of annular channels filled with active liquids and consider the topological density wave propagation in it, as illustrated in Fig. 1(a). For an isolated annulus, a circumferential steady chiral flow of active liquid can emerge spontaneously due to the constituent self-propelled particles and the constraints from the close boundary conditions. Such a chiral flow leads to spontaneous TRS breaking, resulting in nonreciprocal propagation of density waves in topological active-liquid metamaterials without external drives [35]. In the nonreciprocal active-liquid network model, as shown in Figs. 1(a) and 1(b), however, each annulus has three opening ports, and any two adjacent annuli are coupled by a straight link tube. The steady chiral flow within each annulus may leak into its neighboring ones because of these openings, leading to the exchange of active liquid flows in different annuli. This raises a fundamental question as to whether the global uniform steady chiral flow still can survive in each annulus in the presence of opening ports. The answer is affirmative, which can be confirmed by the particle-based numerical simulation of the dynamics of the active-liquid networks (see Note 1 and movie in the Supplemental Material [43]).

The collective dynamical behavior of the active liquid in a polar-type interaction is governed by the Toner-Tu equations [35–37,44–47], which read

$$\partial_t \rho + \nabla \cdot (\rho \mathbf{v}) = 0, \tag{1}$$

$$\partial_t \mathbf{v} + \lambda(\mathbf{v} \cdot \nabla)\mathbf{v} = (\alpha - \beta|\mathbf{v}|^2)\mathbf{v} - \frac{c^2}{\rho_0}\nabla\rho + \gamma\nabla^2\mathbf{v}, \tag{2}$$

where c is the sound speed, $\rho(\mathbf{r}, t)$ is the density of the active liquid, and $\mathbf{v}(\mathbf{r}, t)$ is the local average of the velocities of the self-propelled particles. α and β are the Landau coefficients used to model the spontaneous breaking of the rotational symmetry and here we assume $\lambda = 0.8$, and γ is the diffusive coefficient. For the case of $\alpha > 0$, the Toner-Tu equations result in an ordered phase of the system with $\mathbf{v}$ having a nonzero magnitude $\sqrt{\alpha/\beta}$, as shown by the steady-state chiral flows (thick red arrows) in Fig. 1(b). We consider the fluctuations of the density ($\delta\rho = \rho - \rho_0$) and velocity ($\delta\mathbf{v} = \mathbf{v} - \mathbf{v}_0$) field of the steady state (with ρ_0 and $\mathbf{v}_0$ being the steady-state values) and neglect their second-order contributions and the diffusive term. In the limit of $v_0/c \ll 1$ and assuming an oscillating solution $\delta\tilde{\rho}e^{i\omega t}$ of the density wave, the linearized Toner-Tu equations can be deformed into the Schrödinger-like equation (see Note 2 in the Supplemental Material [43]):

$$(\nabla - i\mathbf{A})^2\, \delta\tilde{\rho} = \frac{\omega^2}{c^2}\, \delta\tilde{\rho}, \tag{3}$$

where $\mathbf{A} = \omega(\lambda + 1)\mathbf{v}_0/(2c^2)$ is the effective vector potential dependent on the steady-state velocity v_0. The spontaneous chiral flow in the annuli analogously contributes an effective magnetic field to the active-liquid networks to break the TRS. On the other hand, in each link tube between two adjacent annuli, the net effective vector potential should be zero since there exist two opposite flows (see Note 1 in the Supplemental Material [43]).

The density waves propagating in the topological active-liquid networks can be well described by a nonreciprocal scattering network model. Due to the spontaneous chiral flow, each annular channel can be regarded as a three-port nonreciprocal circulator described by a 3×3 unitary scattering matrix. For each circulator, the output (denoted as $|a\rangle$) and input (denoted as $|c\rangle$) waves at three ports are related by a unitary scattering matrix S_0 through $|a\rangle = S_0|c\rangle$. The output waves that leave a circulator will turn into the input waves of the neighboring circulator after traveling a distance l along the coupling tubes. These coupling tubes are termed phase links since they generate a phase delay $\phi = \exp(\pm ik_0 l)$ between two neighboring circulators. The density waves propagating in an infinite honeycomb network can be described by a Bloch equation [27,48–51]

$$S(\mathbf{k})\,|c\,(\mathbf{k})\rangle = e^{-i\phi}\,|c\,(\mathbf{k})\rangle, \tag{4}$$

where $\mathbf{k}$ represents the wave vector, $S(\mathbf{k})$ is a 6×6 unitary matrix obtained by assembling the scattering matrices of two neighboring circulators in a unit cell, and $|c(\mathbf{k})\rangle$ represents the Bloch modes that propagate in the honeycomb network. Note that $S(\mathbf{k})$ is parameterized by the inner radius r of the annulus and the particle speed v_0. This nonreciprocal scattering network described by a unitary matrix $S(\mathbf{k})$ can be mapped onto the Floquet eigenproblem of a periodically driven lattice, with the phase delay ϕ playing the role of the quasienergy [52,53].

We then use the model of Eq. (4) to explore the phase diagram of the topological active-liquid network on the (v_0, r) plane, as shown in Fig. 1(c). The colors represent the reflection coefficients at each port of the circulator. The phase diagram reveals three distinct phases: the CI phase with Chern CESs and nonzero Chern number for $|R| > 1/3$, the topological phase transition with quasienergy band gaps ② and ⑤ closing at $|R| = 1/3$, and the AFI phase with zero Chern number but still supporting anomalous nonreciprocal topological edge states for $|R| < 1/3$. We confirm the topological nature of these phases by calculating their winding numbers and Chern numbers (see Note 3 in the Supplemental Material [43]). Furthermore, although our network geometry resembles those in earlier works [9,23], the AFI phase has not been explored in those studies because their frequency-based framework does not exhibit Floquet band structures. By directly solving Eq. (4), we obtain bulk band structures of the nonreciprocal active-liquid network (cyan dots) with different particle speeds v_0 at $r = 0.1271a$ for the AFI phase ($v_0 = 0.0023c$), the topological phase transition phase ($v_0 = 0.0035c$), and the CI phase ($v_0 = 0.0049c$), respectively, as shown in Figs. 1(d)–1(f), in which two band gaps (② and ⑤) close and then reopen, implying the occurrence of a topological phase transition, while the other four band gaps (①, ③, ④, and ⑥) always keep opening. The color map represents the results obtained by solving Eq. (3) using the commercial finite element software COMSOL Multiphysics (see Note 4 in the Supplemental Material [43]). The excellent agreement between these two methods indicates that the semianalytical scattering network model is sufficient to describe the topological features of the nonreciprocal active-liquid network (see Note 5 in the Supplemental Material [43]).

Next, we study the topologically protected edge states of the anomalous and Chern phases. We first calculate the band structure of a ribbonlike supercell composed of 20 circulators with periodic boundary conditions (PBCs) along the x direction and open boundary conditions (OBCs) at the top and bottom edges. The calculated edge dispersions of the anomalous and Chern phases are shown in Figs. 2(a) and 2(c), respectively, in which the dotted lines and the background color represent the results obtained from the model of Eq. (4) and the finite element simulations, respectively. It can be seen that both the AFI and CI phases exhibit CESs propagating along the top (yellow dots) and bottom (cyan dots) edges. The main contrast is that the anomalous CESs exist in every quasienergy band gap, while the Chern CESs only exist in the four band gaps (①, ③, ④, and ⑥) without a topological phase transition. Figures 2(b) and 2(d) show the eigenmode

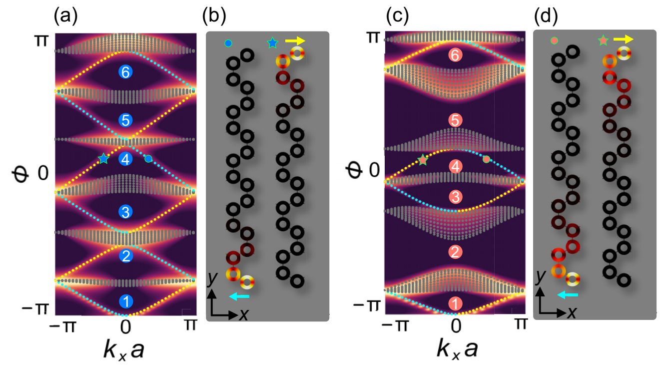

FIG. 2. Anomalous and Chern edge states of the topological active-liquid network. (a) Band structure of a ribbonlike supercell with PBCs in the x direction and OBCs at the top and bottom. The low-reflection case is in the AFI phase, featuring anomalous nonreciprocal topological edge states spanning all quasienergy band gaps marked with numbers. (b) The density wave intensity distributions of the AFI edge states correspond to the blue star and blue circle in panel (a). The yellow and cyan arrows indicate the propagation directions of the AFI edge states. (c), (d) The same as in panels (a) and (b), but for the CI edge states. Note that the CI edge states are absent in band gaps ② and ⑤.

profiles of the AFI and CI CESs corresponding to the blue star and blue circle in Fig. 2(a) and pink star and pink circle in Fig. 2(c), respectively. The cyan and yellow arrows indicate the propagation direction of the CESs. Note that while CESs can be supported by both the AFI and CI phases, there exists a significant difference between their boundary localization strength, which will further lead to different localization levels of the chiral edge modes and the corner skin modes in a non-Hermitian active-liquid network, as we will discuss later.

We then examine the topological robustness of the nonreciprocal anomalous and Chern edge states. Since the AFI phase has flatter bulk bands and larger band gaps than the CI phase and hosts anomalous topological edge states in every quasienergy band gap, it can be intuitively expected that the anomalous nonreciprocal topological edge states should be more robust to disorder than the Chern ones. To verify this prediction, we introduce random disorder to the particle speed and inner radius of the circulator in a finite rectangular active-liquid network. We define Δ_S as the degree of disorders (see Note 6 in the Supplemental Material [43]). For each Δ_S varies from 0% to 100%, the average edge transmissions of the AFI (blue line) and CI (pink line) phases for 100 realizations of the disorder are calculated and plotted in Fig. 3(a), in which the solid lines represent the ensemble average value of the edge transmission, and the dashed lines are the first and last quartiles. When there is no disorder ($\Delta_S = 0$), both the AFI and CI phases exhibit high transmission because their CESs are unperturbed. As Δ_S increases from 0% to 100%, the average transmission of the Chern edge states (pink line) drops quickly. In stark contrast, the transmission of anomalous nonreciprocal topological edge states (blue line) exhibits a different behavior, remaining near 90% even when Δ_S reaches 100% (fully random case). This phenomenon can be further confirmed by the corresponding density wave intensity

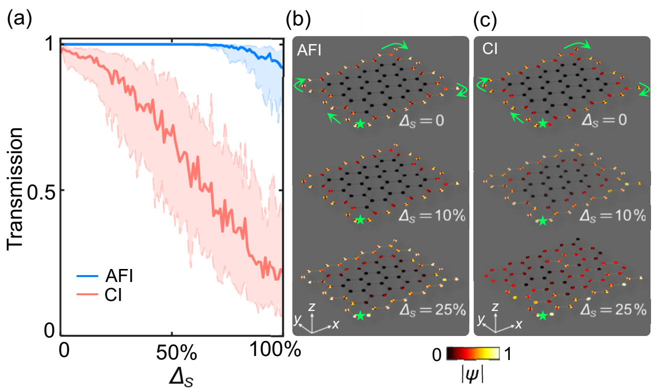

FIG. 3. Comparison of the robustness of AFI and CI edge states against disorder. (a) Transmission of the AFI (blue line) and CI (pink line) edge states with randomly generated (v_0, r). The solid lines represent the transmission averaged over 100 realizations of random disorder, and the dashed lines are the first and last quartiles. Δ_S is the degree of the disorder. Density wave intensity distributions of (b) the AFI and (c) CI phases under different disorder strengths.

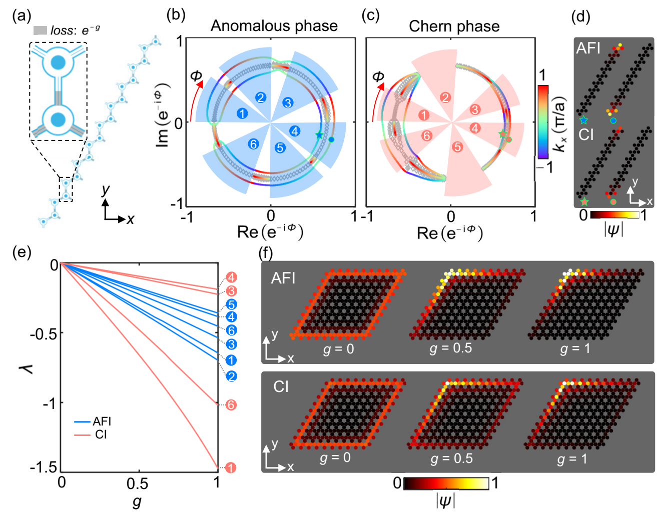

FIG. 4. Non-Hermitian topological active-liquid network. (a) Schematic of the supercell of a non-Hermitian topological active-liquid network with lossy links (shaded region), g represents the loss factor. Complex energy spectra of the (b) anomalous and (c) Chern phases for x-PBC/y-OBC (color curves) and double OBCs (gray diamonds). The blue (pink) sectors marked with numbers indicate anomalous (Chern) quasienergy band gaps, and the polar angles represent the real parts of the minus quasienergy $-\phi$. The red arrow represents the direction of increasing ϕ from $-\pi$. The loss factor $g = 1$. (d) Intensity distributions of the eigenmode of the non-Hermitian AFI and CI phases with x-PBC/y-OBC marked by stars and dots in panels (b) and (c), respectively. (e) The average decay coefficients of the non-Hermitian AFI (blue lines) and CI (pink lines) eigenmodes along the edge as a function of g in different quasienergy band gaps marked with numbers. (f) Intensity distributions of the eigenmode of the non-Hermitian AFI and CI phases with double OBCs and fixed $\phi = \pi/8$ in gap ④ under different loss factors g.

distributions of the anomalous and Chern phases with different disorders Δ_S, as shown in Figs. 3(b) and 3(c). These results demonstrate that the anomalous nonreciprocal edge states of the topological active-liquid network exhibit superior robustness than the Chern ones under the fluctuations of particle speed and the inner radii of the circulator.

III. CHERN AND ANOMALOUS EDGE STATES IN A NON-HERMITIAN ACTIVE-LIQUID NETWORK

Next, we consider a non-Hermitian topological active-liquid network by introducing a dissipative term in Eq. (2). As illustrated in the inset of Fig. 4(a), one annulus of each unit cell includes a loss e^{-g} indicated by the gray region. In this case, both the AFI and CI edge states will be gradually localized to the corner by the NHSE [40,41], forming exotic corner skin modes. To demonstrate this unique phenomenon, we study the supercell shown in Fig. 4(a), which has PBCs along the x direction and OBCs in the y direction ("x-PBC/y-OBC"). Figures 4(b) and 4(c) show the complex quasienergy spectra of the supercell for the anomalous and Chern phases, respectively, and the blue (pink) sectors marked by numbers represent the quasienergy band gaps of the anomalous (Chern) phase. Note that in Figs. 4(b) and 4(c), we adopt $e^{-i\phi}$ as the quasienergy instead of ϕ since the real part of ϕ has a period of 2π (see Note 7 in the Supplemental Material [43]) [54]. It can be seen that, as k_x sweeps through the one-dimensional Brillouin zone of the supercell, the chiral edge modes of both the AFI and CI phases form spectral loops (colored curves) on the complex plane, producing nonzero point-gap winding numbers that can be calculated using the formula (see Note 7 in the Supplemental Material [43]) [40,55,56]

$$\nu_\alpha(\phi_0) = \int_{BZ} \frac{dk_\alpha}{2\pi} \frac{d}{dk_\alpha} \arg[e^{-i\phi(k_\alpha)} - e^{-i\phi_0}], \tag{5}$$

where $\alpha = x, y$ indicates the direction along which PBCs are imposed on the supercell and ϕ_0 is a reference quasienergy within the loop. The point-gap winding number gives rise to the localization of the anomalous and Chern edge states by the NHSE and its sign determines the localization direction of the edge states to the corners. One can define the modes with larger (smaller) imaginary part quasienergy as "gain" (loss) modes that are confined at G (L)-type edge. Figure 4(d) shows the intensity distributions of the "gain" (loss) modes localized at the lower (upper) boundary of the AFI and CI phases with fixed $\phi = \pi/8$.

We now consider a finite rhombic active-liquid network composed of 10 × 10 unit cells with OBCs along both the x and y directions ("double OBCs") to examine the AFI and Chern edge states under non-Hermitian perturbations. The calculated complex quasienergy spectra of this finite rhombic network in the AFI and CI phases (gray diamonds) are plotted in Figs. 4(b) and 4(c), respectively. Both the anomalous and Chern edge states will be localized at the corner and transition to the corner skin modes via NHSE. Since the corner skin modes have exponential eigenfunction distributions along the edges, thus we can define $|\psi_{p,n}| \propto e^{\lambda}_{p,n}$, where $\lambda_{p,n}$ is the decay coefficient and $|\psi_{p,n}|$ is the amplitude at the nth site along the p-type edges with p representing G (L). Note that the left and bottom (right and upper) boundaries of the finite non-Hermitian nonreciprocal topological networks support "gain" (loss) modes. In Fig. 4(e), we plot the mean decay coefficients

($\lambda = \sum_{i=1}^{3} \frac{\lambda_{G,i}+\lambda_{L,i}}{3\times 2}$) of three midgap eigenmodes of AFI (blue lines) or CI (pink lines) along two types of edges in different quasienergy band gaps as a function of the loss factor g. The steeper the slope of the mean decay coefficients to the loss factor g, the more vulnerable the edge states are to the non-Hermitian perturbations. Counterintuitively, the superior robustness of AFI edge states over the CI ones does not persist in the non-Hermitian case. In contrast, the CI edge states in quasienergy band gaps ③ and ④ (① and ⑥) are more (less) robust than the AFI edge states in all six band gaps to the non-Hermitian perturbations. That is because the robustness of the AFI and CI edge states against non-Hermitian perturbations depends on the boundary localization strength of the edge states with $g = 0$. The stronger boundary localization of the edge states at $g = 0$, the weaker robustness against the non-Hermitian perturbations (see Note 8 in the Supplemental Material [43]). The eigenmode intensity distributions of the non-Hermitian AFI phase (upper panel) and CI phase (lower panel) both in band gap ④ under different loss factors g are plotted in Fig. 4(f), from which we can see that both the AFI and CI edge states are gradually localized to the upper left corner by the NHSE with increasing loss factors g. Remarkably, with the same nonzero loss factors g, the AFI corner skin modes (upper panel) exhibit stronger localization than those of the CI ones (lower panel), indicating that the CI edge states are more robust than the AFI ones in band gap ④ against the non-Hermitian perturbations, which is different from the Hermitian case.

IV. CONCLUSIONS

In summary, we have theoretically extended anomalous nonreciprocal topological networks to topological active matter systems and demonstrated anomalous and Chern CESs in topological active-liquid networks with spontaneous TRS breaking in the absence of any external drives. We show that the anomalous nonreciprocal topological edge states exhibit superior robustness against Hermitian disorders than the Chern ones. However, such superior robustness does not hold in the presence of non-Hermitian perturbations induced by dissipation, and both the anomalous and Chern CESs transition to corner skin modes by the NHSE. Counterintuitively, the Chern CESs in some quasienergy band gaps are even more robust than the anomalous ones against non-Hermitian perturbations, exhibiting different behaviors from the Hermitian case. Since experiments on the dynamics of active fluids have been demonstrated in coupled annular channels [57] and large-scale networks [58], we envision that the unique topological effects of this work can also be observed in similar systems. Our findings may have potential applications for the manipulation of sound in both Hermitian and non-Hermitian topological active-liquid network systems.

ACKNOWLEDGMENTS

Z.G. acknowledges the funding from the National Natural Science Foundation of China under Grants No. 62361166627 and No. 62375118, Guangdong Basic and Applied Basic Research Foundation under Grant No. 2024A1515012770, Shenzhen Science and Technology Program under Grants No. 20220815111105001 and No. 202308073000209, and High-level Special Funds under Grant No. G03034K004. L.Y. acknowledges the funding from Natural Science Foundation of Chongqing under Grant No. CSTB2025NSCQ-GPX0776. The authors acknowledge the helpful discussions with Anton Souslov (University of Cambridge), Kazuki Sone (University of Tsukuba), and Yaohua Li (Tsinghua University).

DATA AVAILABILITY

The data that support the findings of this article are not publicly available upon publication because it is not technically feasible and/or the cost of preparing, depositing, and hosting the data would be prohibitive within the terms of this research project. The data are available from the authors upon reasonable request.

[1] D. J. Thouless, M. Kohmoto, M. P. Nightingale, and M. den Nijs, Quantized Hall conductance in a two-dimensional periodic potential, Phys. Rev. Lett. **49**, 405 (1982).

[2] C. L. Kane and E. J. Mele, Z_2 topological order and the quantum spin Hall effect, Phys. Rev. Lett. **95**, 146802 (2005).

[3] M. Z. Hasan and C. L. Kane, *Colloquium*: Topological insulators, Rev. Mod. Phys. **82**, 3045 (2010).

[4] F. D. M. Haldane and S. Raghu, Possible realization of directional optical waveguides in photonic crystals with broken time-reversal symmetry, Phys. Rev. Lett. **100**, 013904 (2008).

[5] A. B. Khanikaev, S. Hossein Mousavi, W.-K. Tse, M. Kargarian, A. H. MacDonald, and G. Shvets, Photonic topological insulators, Nat. Mater. **12**, 233 (2013).

[6] M. C. Rechtsman, J. M. Zeuner, Y. Plotnik, Y. Lumer, D. Podolsky, F. Dreisow, S. Nolte, M. Segev, and A. Szameit, Photonic Floquet topological insulators, Nature (London) **496**, 196 (2013).

[7] H. Xue, Y. Yang, and B. Zhang, Topological acoustics, Nat. Rev. Mater. **7**, 974 (2022).

[8] Z. Yang, F. Gao, X. Shi, X. Lin, Z. Gao, Y. Chong, and B. Zhang, Topological acoustics, Phys. Rev. Lett. **114**, 114301 (2015).

[9] Y. Ding, Y. Peng, Y. Zhu, X. Fan, J. Yang, B. Liang, X. Zhu, X. Wan, and J. Cheng, Experimental demonstration of acoustic Chern insulators, Phys. Rev. Lett. **122**, 014302 (2019).

[10] A. Darabi, M. Collet, and M. J. Leamy, Experimental realization of a reconfigurable electroacoustic topological insulator, Proc. Natl. Acad. Sci. USA **117**, 16138 (2020).

[11] S. D. Huber, Topological mechanics, Nat. Phys. **12**, 621 (2016).

[12] L. M. Nash, D. Kleckner, A. Read, V. Vitelli, A. M. Turner, and W. T. M. Irvine, Topological mechanics of gyroscopic metamaterials, Proc. Natl. Acad. Sci. USA **112**, 14495 (2015).

[13] N. P. Mitchell, L. M. Nash, D. Hexner, A. M. Turner, and W. T. M. Irvine, Amorphous topological insulators constructed from random point sets, Nat. Phys. **14**, 380 (2018).

[14] C. H. Lee, S. Imhof, C. Berger, F. Bayer, J. Brehm, L. W. Molenkamp, T. Kiessling, and R. Thomale, Topolectrical circuits, Commun. Phys. **1**, 39 (2018).

[15] J. Dong, V. Juričić, and B. Roy, Topolectric circuits: Theory and construction, Phys. Rev. Res. **3**, 023056 (2021).
[16] T. Kotwal, F. Moseley, A. Stegmaier, S. Imhof, H. Brand, T. Kießling, R. Thomale, H. Ronellenfitsch, and J. Dunkel, Active topolectrical circuits, Proc. Natl. Acad. Sci. USA **118**, e2106411118 (2021).
[17] G. Xu, Y. Yang, X. Zhou, H. Chen, A. Alù, and C.-W. Qiu, Diffusive topological transport in spatiotemporal thermal lattices, Nat. Phys. **18**, 450 (2022).
[18] H. Hu *et al.*, Observation of topological edge states in thermal diffusion, Adv. Mater. **34**, 2202257 (2022).
[19] C. He, X. Ni, H. Ge, X.-C. Sun, Y.-B. Chen, M.-H. Lu, X.-P. Liu, and Y.-F. Chen, Acoustic topological insulator and robust one-way sound transport, Nat. Phys. **12**, 1124 (2016).
[20] J. Lu, C. Qiu, L. Ye, X. Fan, M. Ke, F. Zhang, and Z. Liu, Observation of topological valley transport of sound in sonic crystals, Nat. Phys. **13**, 369 (2017).
[21] J.-W. Dong, X.-D. Chen, H. Zhu, Y. Wang, and X. Zhang, Valley photonic crystals for control of spin and topology, Nat. Mater. **16**, 298 (2017).
[22] F. D. M. Haldane, Model for a quantum Hall effect without Landau levels: Condensed-matter realization of the "parity anomaly," Phys. Rev. Lett. **61**, 2015 (1988).
[23] A. B. Khanikaev, R. Fleury, S. H. Mousavi, and A. Alù, Topologically robust sound propagation in an angular-momentum-biased graphene-like resonator lattice, Nat. Commun. **6**, 8260 (2015).
[24] X. Ni, C. He, X.-C. Sun, X. Liu, M.-H. Lu, L. Feng, and Y.-F. Chen, Topologically protected one-way edge mode in networks of acoustic resonators with circulating air flow, New J. Phys. **17**, 053016 (2015).
[25] Z. Wang, Y. Chong, J. D. Joannopoulos, and M. Soljačić, Observation of unidirectional backscattering-immune topological electromagnetic states, Nature (London) **461**, 772 (2009).
[26] Z. Zhang, P. Delplace, and R. Fleury, Anomalous topological waves in strongly amorphous scattering networks, Sci. Adv. **9**, eadg3186 (2023).
[27] Z. Zhang, P. Delplace, and R. Fleury, Superior robustness of anomalous non-reciprocal topological edge states, Nature (London) **598**, 293 (2021).
[28] A. Kumar, M. Gupta, and R. Singh, Topological integrated circuits for 5G and 6G, Nat. Electron. **5**, 261 (2022).
[29] H. Qin, Z. Zhang, Q. Chen, Z. Zhang, and R. Fleury, Anomalous-Chern steering of topological nonreciprocal guided waves, Adv. Mater. **36**, 2401716 (2024).
[30] H. Qin, Z. Zhang, Q. Chen, and R. Fleury, Disclination states in nonreciprocal topological networks, Phys. Rev. Res. **6**, 013031 (2024).
[31] Q. Chen, Z. Zhang, H. Qin, A. Bossart, Y. Yang, H. Chen, and R. Fleury, Anomalous and Chern topological waves in hyperbolic networks, Nat. Commun. **15**, 2293 (2024).
[32] S. Shankar, A. Souslov, M. J. Bowick, M. C. Marchetti, and V. Vitelli, Topological active matter, Nat. Rev. Phys. **4**, 380 (2022).
[33] S. Ramaswamy, Active fluids, Nat. Rev. Phys. **1**, 640 (2019).
[34] N. Lu-Hui, Z. Xue, Y. Ming-Cheng, Z. Ning, L. Peng, and P. Yi, Effect of passive particle shape on effective force in active bath, Acta Phys. Sin. **73**, 158202 (2024).
[35] A. Souslov, B. C. van Zuiden, D. Bartolo, and V. Vitelli, Topological sound in active-liquid metamaterials, Nat. Phys. **13**, 1091 (2017).
[36] K. Sone and Y. Ashida, Anomalous topological active matter, Phys. Rev. Lett. **123**, 205502 (2019).
[37] S. Shankar, M. J. Bowick, and M. C. Marchetti, Topological sound and flocking on curved surfaces, Phys. Rev. X **7**, 031039 (2017).
[38] A. Souslov, K. Dasbiswas, M. Fruchart, S. Vaikuntanathan, and V. Vitelli, Topological waves in fluids with odd viscosity, Phys. Rev. Lett. **122**, 128001 (2019).
[39] Q. Yang, H. Zhu, P. Liu, R. Liu, Q. Shi, K. Chen, N. Zheng, F. Ye, and M. Yang, Topologically protected transport of cargo in a chiral active fluid aided by odd-viscosity-enhanced depletion interactions, Phys. Rev. Lett. **126**, 198001 (2021).
[40] G.-G. Liu *et al.*, Localization of chiral edge states by the non-Hermitian skin effect, Phys. Rev. Lett. **132**, 113802 (2024).
[41] Y. Li, C. Liang, C. Wang, C. Lu, and Y.-C. Liu, Gain-loss-induced hybrid skin-topological effect, Phys. Rev. Lett. **128**, 223903 (2022).
[42] N. Okuma, K. Kawabata, K. Shiozaki, and M. Sato, Topological origin of non-Hermitian skin effects, Phys. Rev. Lett. **124**, 086801 (2020).
[43] See Supplemental Material at http://link.aps.org/supplemental/10.1103/rvkr-7mr2 for the derivation of theoretical equations, verification of theoretical models, and simulation videos of active particles.
[44] M. C. Marchetti, J. F. Joanny, S. Ramaswamy, T. B. Liverpool, J. Prost, M. Rao, and R. A. Simha, Hydrodynamics of soft active matter, Rev. Mod. Phys. **85**, 1143 (2013).
[45] J. Toner and Y. Tu, Long-range order in a two-dimensional dynamical XY model: How birds fly together, Phys. Rev. Lett. **75**, 4326 (1995).
[46] J. Toner and Y. Tu, Flocks, herds, and schools: A quantitative theory of flocking, Phys. Rev. E **58**, 4828 (1998).
[47] J. Toner, Y. Tu, and S. Ramaswamy, Hydrodynamics and phases of flocks, Ann. Phys. **318**, 170 (2005).
[48] G. Q. Liang and Y. D. Chong, Optical resonator analog of a two-dimensional topological insulator, Phys. Rev. Lett. **110**, 203904 (2013).
[49] P. Delplace, M. Fruchart, and C. Tauber, Phase rotation symmetry and the topology of oriented scattering networks, Phys. Rev. B **95**, 205413 (2017).
[50] R. Fleury, D. L. Sounas, C. F. Sieck, M. R. Haberman, and A. Alù, Sound isolation and giant linear nonreciprocity in a compact acoustic circulator, Science **343**, 516 (2014).
[51] M. Pasek and Y. D. Chong, Network models of photonic Floquet topological insulators, Phys. Rev. B **89**, 075113 (2014).
[52] M. S. Rudner, N. H. Lindner, E. Berg, and M. Levin, Anomalous edge states and the bulk-edge correspondence for periodically driven two-dimensional systems, Phys. Rev. X **3**, 031005 (2013).
[53] M. S. Rudner and N. H. Lindner, Band structure engineering and non-equilibrium dynamics in Floquet topological insulators, Nat. Rev. Phys. **2**, 229 (2020).
[54] H. Gao, H. Xue, Z. Gu, L. Li, W. Zhu, Z. Su, J. Zhu, B. Zhang, and Y. D. Chong, Anomalous Floquet non-Hermitian skin effect in a ring resonator lattice, Phys. Rev. B **106**, 134112 (2022).

[55] Z. Gong, Y. Ashida, K. Kawabata, K. Takasan, S. Higashikawa, and M. Ueda, Topological phases of non-Hermitian systems, Phys. Rev. X **8**, 031079 (2018).

[56] D. S. Borgnia, A. J. Kruchkov, and R.-J. Slager, Non-Hermitian boundary modes and topology, Phys. Rev. Lett. **124**, 056802 (2020).

[57] J. Hardoüin, J. Laurent, T. Lopez-Leon, J. Ignés-Mullol, and F. Sagués, Active microfluidic transport in two-dimensional handlebodies, Soft Matter **16**, 9230 (2020).

[58] C. Jorge, A. Chardac, A. Poncet, and D. Bartolo, Active hydraulics laws from frustration principles, Nat. Phys. **20**, 303 (2024).